

Advanced Non-Destructive Testing Techniques for Welded Joint Repairs: A Case Study on Improving Inspection Reliability and Structural Integrity Assessment

Mohammadebrahim Bajgholi ^a, Gilles Rousseau ^{b*}, Denis Thibault ^b, Simon Francoeur ^c

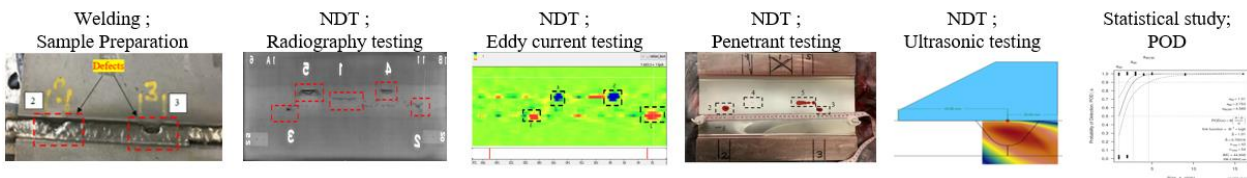
^a Department of Mechanical Engineering, École de Technologie Supérieure, Montréal, Canada

^b Institut de Recherche d'Hydro-Québec (IREQ), Varennes, Canada

^c NDT Applications Specialist, Nucleom, Québec, Canada

*Corresponding author: rousseau.gillesa@hydroquebec.com

Graphical abstract



Abstract

This study evaluates advanced Non-Destructive Testing (NDT) techniques for detecting flaws in welded repairs of martensitic stainless steel plates, with a focus on Francis turbine runners. Phased Array Ultrasonic Testing (PAUT), Total Focusing Method (TFM), and Eddy Current Array (ECA) technologies were examined to assess repair integrity and identify flaws such as lack of fusion (LOF). The research compares surface and volumetric inspection methods across filler materials, including 410NiMo and 309L alloys, with an emphasis on shallow repairs (<6 mm). Conventional surface inspection methods, like Penetrant testing (PT), were insufficient for detecting subsurface flaws, especially in geometrically complex components. Subsurface flaws missed by PT were successfully identified using ECA and PAUT, underscoring the limitations of conventional techniques. PAUT achieved near-surface analysis with nearly 100% detection rates for deeper flaws, while ECA excelled at identifying partial LOF in shallow repairs. These findings highlight the necessity of integrating advanced NDT techniques to ensure the structural integrity of critical components, particularly in high-stress applications such as turbine runners. This study advances reliable inspection practices, addressing the limitations of surface methods and improving the detection of critical flaws in repaired welds.

Keywords:

Non-Destructive Testing, PAUT, TFM, Eddy Current Array, PT, Flaws, Welded Joint Repairs.



1. Introduction

The inspection of repair welds in turbine runners is crucial for ensuring the long-term reliability and operational safety of power generation systems. Turbine runners, which convert hydraulic energy into mechanical energy, are subjected to high stresses during operation, making them particularly susceptible to defects in welded repairs. In hydropower plants, maintaining the structural integrity of these components is vital, as failures can lead to significant operational downtime, expensive repairs, and, in severe cases, catastrophic disasters [1-2]. To mitigate these risks, Non-Destructive Testing (NDT) methods play a pivotal role in assessing the quality of repairs without compromising the material [3]. On-site repairs typically use austenitic stainless filler metals (e.g., 309L) to avoid the risk of cold cracking associated with martensitic filler metals. Shallow repairs, typically involving weld excavations of less than 6 mm, are commonly inspected using surface techniques such as dye penetrant testing (PT). However, surface-based methods like PT have well-documented limitations, especially when it comes to detecting subsurface defects such as lack of fusion (LOF) in critical areas like the high-stress zones of Francis turbine runners. Studies have shown that surface inspection methods frequently fail to identify hidden flaws, which can compromise the structural integrity of the component and lead to operational failures [4,5]. To overcome the limitations of traditional surface inspection methods, more advanced NDT techniques, such as Eddy Current Testing (ECT) and Phased Array Ultrasonic Testing (PAUT), have been developed [6]. ECT, particularly when using Eddy Current Array (ECA) technology, is effective in detecting surface-connected and near-surface defects, providing detailed insights into weld quality in non-ferromagnetic materials such as 309L [7, 8]. Similarly, PAUT, when combined with the Total Focusing Method (TFM), enables detailed volumetric analysis of welds, allowing for the detection of subsurface defects often missed by surface techniques. These advanced methods are especially beneficial for the complex geometries of Francis turbine blades, where conventional ultrasonic inspections struggle due to geometric irregularities and material reflections [9, 10].

Despite advancements in NDT technology, research gaps remain regarding the specific effectiveness of PAUT and ECA in detecting critical defects, such as lack of fusion (LOF), in shallow welded repairs of martensitic stainless steel turbine runner plates. While previous studies have primarily focused on deeper repairs or simpler geometries, there is limited understanding of

how these techniques perform in shallow repairs within complex structures. This study seeks to address this gap by evaluating the performance of PAUT and ECA in detecting LOF in shallow welded repairs and comparing their effectiveness to conventional surface inspection techniques.

The research focuses on welded repairs made using 309L (typically used for on-site repair) and martensitic 410NiMo filler materials (typically used in the shop during manufacturing or major rehabilitation). The findings will contribute to the development of more reliable methods for ensuring the structural integrity of turbine runners and provide valuable insights for improving inspection practices in high-stress areas of welded structures. In the following sections, this paper will introduce the relevant NDT techniques, followed by a comparison of their effectiveness in detecting LOF in shallow turbine runner repairs. The results of this study will offer guidance on enhancing the reliability of hydropower generation equipment and inform best practices for inspection protocols in similar applications.

2. Methodology

The methodology employed in this study is illustrated in the flowchart presented in Figure 1. It was designed to evaluate a range of parameters that could influence inspection outcomes. The primary objective was to assess the effectiveness of Phased Array Ultrasonic Testing (PAUT) and Eddy Current Array (ECA) technologies in inspecting repairs performed using 309L or 410NiMo filler metal on martensitic steel plates.

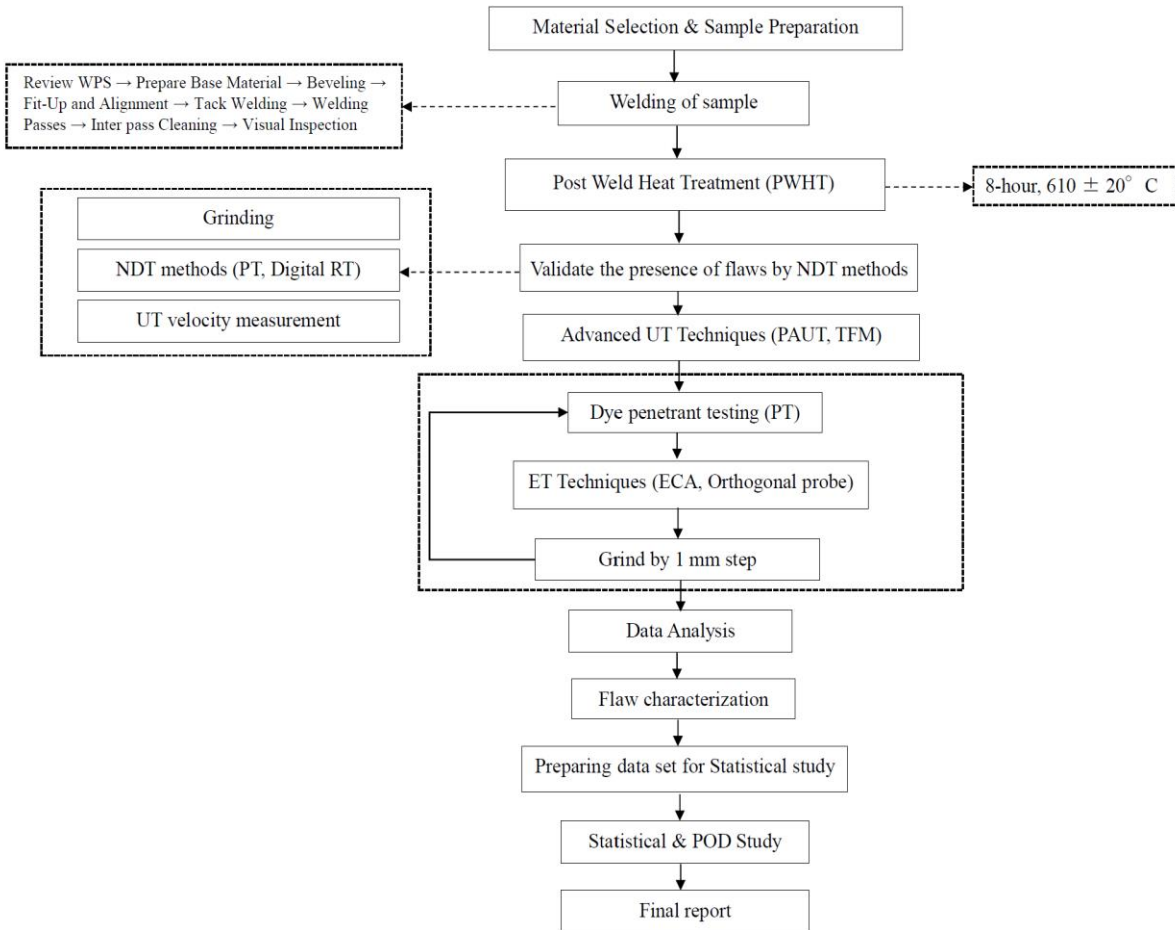


Figure 1. Workflow for current study (Note: PWHT not applied to 410 plates with 309L).

2.1. Sample Preparation

Two types of martensitic steels were selected for this study: (a) 410 hot-rolled and (b) 415 hot-rolled. The 415 steel has the same chemical composition as CA6NM martensitic steel, and its ultrasonic properties have been well-documented in previous studies. The 410 steel was chosen for its availability, widespread use across various industries, and similar microstructure, allowing for the exploration of scenarios where its ultrasonic properties differ from those of 415. The 410 plates used in this project exhibit ultrasonic anisotropy, adding complexity to the inspection process [1,4,9].

The repairs were geometrically simplified by machining a groove across the full width of the plates, which was subsequently filled with weld beads. While this process is more similar to hard-facing than local repair, it effectively introduced a significant number of defects and facilitated data collection through encoded linear scanning. This approach enabled efficient inspection,

volumetric data recording, and post-processing to display results as projections on the plate surfaces.

The design and production of the plates were a collaborative effort between IREQ and the Québec Metallurgy Center (CMQ). CMQ supplied four 410 stainless steel plates, while IREQ provided a 415 rolled steel block. Each plate featured a V-shaped groove profile with a 30° bevel angle. The groove depth was 12 mm for the 410 plates and 18 mm for the 415 plates. Five fusion defects were intentionally introduced into each plate by adjusting the welding torch angle and speed to create a lack of bonding with the grooved wall. The defect lengths ranged from 10 to 25 mm and were distributed as follows:

- **Defect #1:** Located in the bottom pass.
- **Defects #2 and #3:** Located in intermediate passes (2nd pass for 410 plates, 3rd pass for 415 plates).
- **Defects #4 and #5:** Located in the final pass.

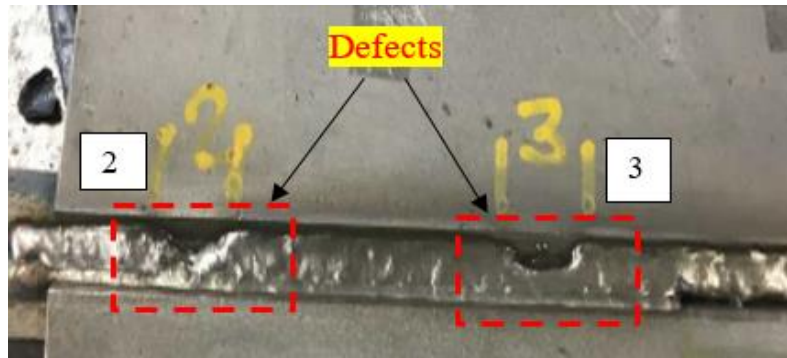


Figure 2. Examples of location of defects #2 and #3 on Plate 309-1.

After welding, the 415 plates were subjected to heat treatment at $610 \pm 20^\circ\text{C}$ for 8 hours. If necessary, the plates were straightened, and the weld beads were trimmed. Notably, near-surface defects in specimen 415/309L cracked during the straightening process, exposing defect #5 at the surface. Subsequently, the plates were subjected to X-ray inspection to verify the presence of

fusion defects, as shown in Figure 3. All 20 expected defects were confirmed, although they were shorter in the 415 specimens. Additionally, some unintentional welding defects were observed.

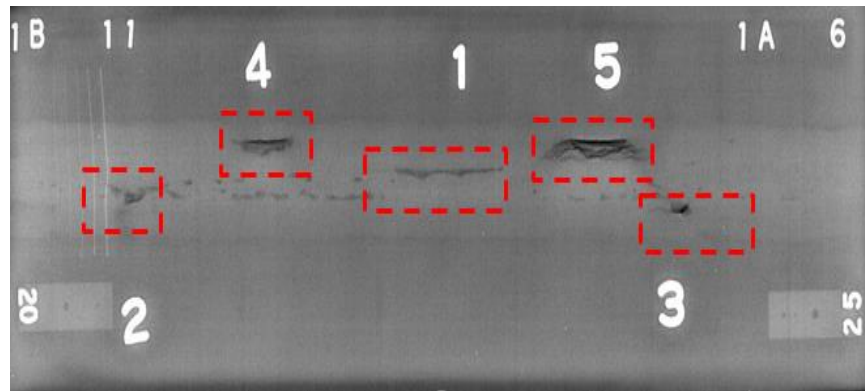


Figure 3. Radiographic Results of Plate 415 with 309L Filler

The inspection was conducted in two phases to validate the presence of flaws:

1. **Ultrasonic Inspection Phase:** In this phase, only ultrasonic array probes were used to inspect the repaired volume.
2. **Destructive Inspection Phase:** This phase involved penetrant testing and eddy current inspections performed during grinding operations, which removed material layer by layer (1 mm at a time) until the indications were excavated. This process enabled accurate dimensioning of all welding defects extending into the plate thickness. Penetrant testing data was used to assess the effectiveness of ultrasonic and eddy current inspections. While flaw length measurements were within the accuracy of penetrant testing, the true height remained uncertain due to the layering process used for excavation.

2.2. Inspection technologies

The following inspection technologies were employed in repair samples:

- a) **Phased Array Ultrasonic Testing (PAUT) and Total Focusing Method (TFM):** Ultrasonic inspections were performed using three array probe techniques that utilized both compressional and shear waves. To maximize flexibility in ultrasonic array configurations, a 64-element transducer was employed, operating at frequencies of 2.25 and 5 MHz. The phased array instrument used was Zetec's Topaz64, equipped with the high-resolution TFM option. Data analysis was conducted using Ultra Vision 3 software, which merged the data

and generated projected views of defects. The primary focus of the inspection was the fusion zone between the groove preparation and the filler metal. Given the plate geometry, inspections were carried out on both sides of the repair, with waves incident normally on the bevel to produce strong echoes returning to the probe (Figure 4).

- **UT Technique #1: PAUT-Compound Scanning:** This technique varied the angle of incidence to generate a fan-shaped beam array, covering angles from 40° to 70° in 1° increments. The range of angles, the number of elements, and the distance from the wedge were determined to ensure full coverage of the region of interest at near-normal incidence with the repair joint.
- **UT Technique #2: PAUT-Linear Scanning:** A fixed angle of incidence of 60° , perpendicular to the groove face, was used. For the 415 plates, two scans were required, and the resulting data files were merged.
- **UT Technique #3: Total Focusing Method (TFM):** Total Focusing Method (TFM) is a data-processing algorithm rather than a conventional beam-forming technique. In this approach, each element in the array was activated sequentially, while all 64 elements continuously received reflected signals [11]. The resulting image depicted ultrasound density, providing a visual representation where voxel colors corresponded to the probability of defect presence.

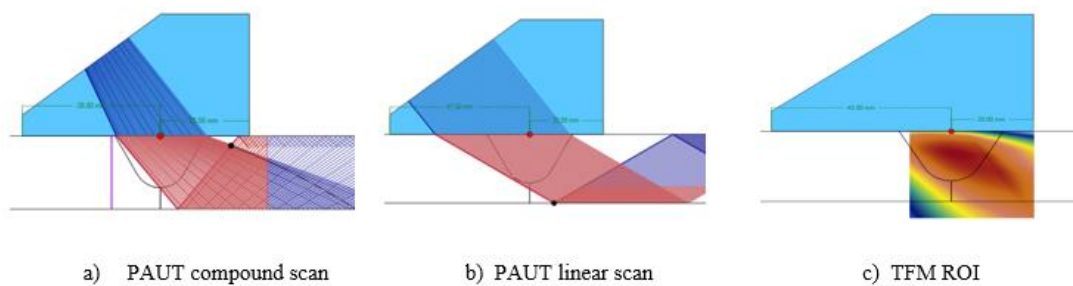


Figure 4. Beam simulation of three ultrasonic array techniques for detecting near-surface fusion defects.

b) Eddy Current Technique: Two eddy current techniques were evaluated.

- **Eddy Current Array (ECA):** Eddy Current Array (ECA) is an advanced non-destructive testing (NDT) technology that uses multiple eddy current coils in a single probe to detect surface and near-surface flaws efficiently. It enhances inspection speed, coverage, and accuracy, making it ideal for detecting cracks, corrosion, and material defects in conductive materials. ECA testing was performed using SGNDT's S2G2 and Zetec's MIZ-21C portable devices. Flexible probes with diameters of 3 mm (75 kHz) and 5 mm (20 kHz) were used. These frequencies were chosen to detect both surface-connected and subsurface defects.
- **Orthogonal Probe:** The orthogonal coil probe was used with the Omniscan ET system, fitted with an 8 mm Olympus probe. This configuration demonstrated high sensitivity to fusion flaws both parallel and perpendicular to the weld axis.

Both ultrasonic and ECA scanning were conducted using encoded linear scanning. The scan direction was aligned parallel to the weld axis, with the probe distance from the weld adjusted to ensure the required coverage. The orthogonal probe was manually positioned using a guide along the weld edge, and discontinuities were recorded where signal indications were detected as shown in figure 5.

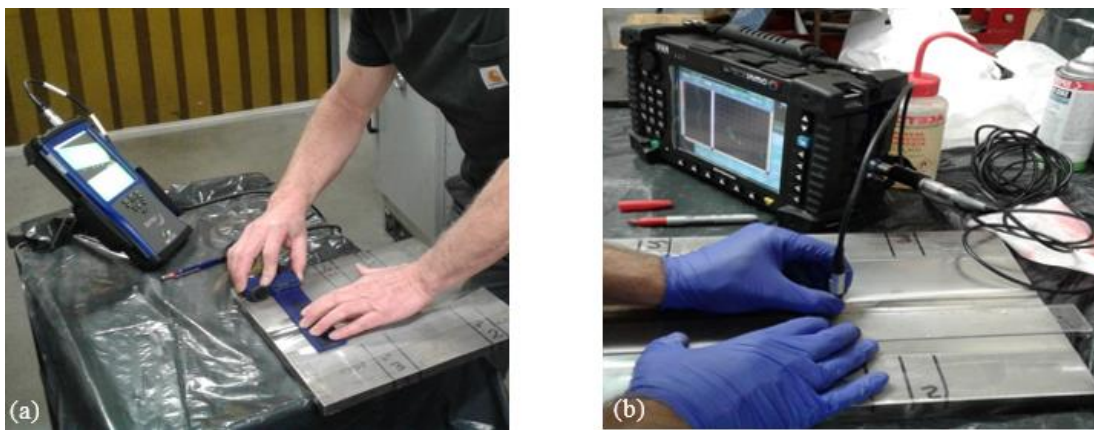


Figure 5. Eddy current testing: (a) ECA Inspection and (b) Orthogonal Probe

c) Penetrant technique (PT):

Penetrant testing (PT) was utilized during the destructive inspection phase to detect surface-connected flaws after each grinding stage and for length measurements. The application of PT was

based on ASTM E165 [12]. A visible red dye penetrant was used with an extractable developer to enhance sensitivity to small and tight defects. Flaw length was measured promptly after it appeared to minimize length-sizing error. The inspector continuously monitored the development process and ensured that only the extremities of the flaw were included in the measurement. The smooth surface finish provided ideal conditions for PT inspection, resulting in accurate length sizing with an estimated error of ± 1 mm.

2.3. Velocity measurement

Initial ultrasonic inspection tests revealed challenges in detecting defects in certain specimens. Velocity measurements were performed using contact shear and compression transducers on the plates and weld coupons, in accordance with ASTM E494 guidelines, as summarized in Table 1. [13]. A comprehensive analysis of sound velocity across various materials revealed that compression wave velocities were relatively consistent, whereas significant variations were observed in shear wave velocities. For shear waves, the 415 plates, 410NiMo filler, and AWS carbon steel blocks exhibited similar velocities of approximately 3230 ± 10 m/s. However, the 309L filler material had a lower velocity of 3130 m/s (3.2% lower), whereas the 410 plates displayed a higher velocity of 3520 m/s (9% higher), with 3% anisotropy between the two primary directions. This difference in velocity may be attributed to a textural effect introduced during rolling; however, this hypothesis was not verified through additional methods. Both the 410 plates and the 410 calibration sample were machined in alignment with the rolling direction (3520 m/s), resulting in consistent velocities along the inspection direction.

Table 1. Ultrasound velocity measurement in various material.

Material	Shear Wave Velocity (m/s)	Compression Wave Velocity (m/s)
Plate 410	3520	5870
Plate 415	3220	5875
309L	3130	5874
410NiMo	3230	5878
Block AWS	3240	5920

3. Discussion and results

3.1. Penetrant Testing (PT)

The PT results were obtained during the destructive phase of the project. As PT serves as a benchmark for comparing other techniques, these results are presented first. It is important to note that layer removal was performed with millimeter precision. The final two layers of the 415 plates were 2 mm thick, as no indications were detected by ultrasound at depths between 10 and 14 mm.

This analysis focuses solely on indications related to the intentional lack of fusion (LOF) flaws created by adjusting the torch angle. Other unexpected defects are excluded from this report. However, some unintended defects are present alongside the LOF flaws and are included in the PT results, as the technician could not distinguish between intentional and unintentional defects. The defect sizes determined by dye penetrant testing are summarized in Table 2. The height of the defects corresponds to the number of layers producing a positive PT result, while the length is the maximum measured at the center of the flaw.

Plates using 309L filler (309-1 and 309-2) exhibited greater deformation compared to those using 410NiMo filler. The lower thermal expansion of 410NiMo and its low-temperature martensitic transformation both lower the welding distortion of the 410NiMo welds. It is assumed that this lower distortion participated in 410NiMo tighter LOF with flaw heights around 1-2 mm. This suggests that ultrasonic detection of flaws in plates 410-1 (plate 410) and 410-2 (plate 415) will be considerably more challenging with smaller and tighter lack of fusion.

It is also important to note that during straightening, lack of fusion indications #4 and #5 in specimen 309-2 cracked. Indication #4 did not reach the surface, while indication #5 produced a wide penetrant indication, as shown in Figure 6.

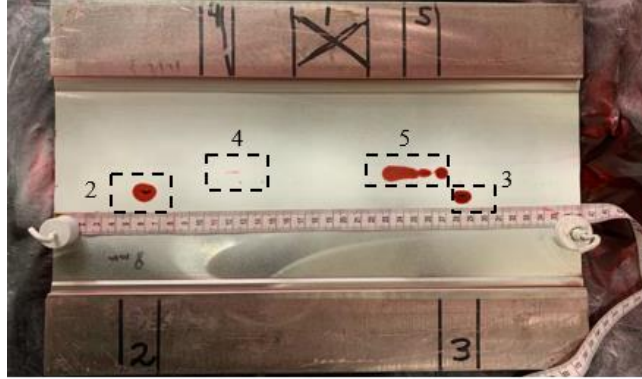


Figure 6. PT of Plate 309-2 at 8 mm Depth.

Table 2. Dimensions of indications according to stratigraphic penetrant testing (height x length) mm.

Sample	Plate	LOF#1	LOF#2	LOF#3	LOF#4	LOF#5
309-1	410	4x55	3x13	5x10	3x10	3x15
410-1	410	3x20	2x9	1x2	1x10	1x12
309-2	415	----	3x9	3x14	9x16*	16x27*
410-2	415	----	2x7	1x18	1x8	2x8
* :Cracked while straightening						
---- : excavation did not reach flaw						

3.2. Eddy Current Inspection (ECI)

The eddy current inspection (ECI) involved three distinct activities conducted during the destructive phase of the project. The techniques employed were as follows:

- Manual orthogonal probe.
- Encoded ECA probe with a 3 mm coil at 75 kHz.
- Encoded ECA probe with a 5 mm coil at 20 kHz.

Inspection of specimens in which both the plate and filler metal were ferromagnetic (i.e., 410 and 415 plates with 410NiMo filler) did not present significant challenges. The scans yielded consistent results, with no discernible boundary between the plate (410 or 415) and the 410NiMo filler metal. The penetration depth at a frequency of 20 kHz was approximately 0.44 mm; however, this value is theoretical, as magnetic permeability and electrical conductivity were not directly measured. The values used were based on experience with Line Core technology, where the relative permeability of steels at 77 kHz is approximately 45, and the nominal conductivity was assumed to be that of 309 steel (1.43 MS/m) [14]. The eddy current inspection of the non-

ferromagnetic 309L material was simpler due to its higher electrical conductivity of 1.43 MS/m, resulting in a penetration depth of approximately 3 mm. At the 309L/415 interface, eddy currents were expected to rise rapidly along the interface and reach a penetration depth of 0.44 mm in the ferromagnetic material. Challenges arose when inspecting specimens with 309L filler material, as the transition between the ferromagnetic plate and the non-ferromagnetic filler produced a strong permeability signal, increasing from 1 to 45. Since the lack of fusion (LOF) defects were located at the boundary between the two materials, the permeability signal overlapped with the defect signal.

To mitigate the permeability effect, two strategies were implemented:

- Orthogonal Probe: A linear scan along the weld axis was conducted. In this configuration, the permeability signal remained constant along the scan axis, and any signal deviation was indicative of a lack of fusion.
- ECA Probe: A linear scan along the weld axis was performed, followed by the application of a median filter to emphasize abrupt variations caused by lack of fusion relative to the averaged permeability signal.

Due to time constraints, the influence of permeability and lack of fusion (LOF) on the eddy current signal was not studied in detail. However, it is reasonable to assume that an optimized coil configuration and frequency could effectively separate these two effects, enabling efficient inspection of 309L/415 repairs for the presence of LOF. The eddy current inspection was performed after each trimming operation, concurrently with penetrant testing. Data collected included the presence or absence of indications, their positions, and lengths. This approach allowed for a direct correlation between the eddy current measurements and penetrant testing results. An example of an ECA C-scan is shown in Figure 7, derived from specimen 309-1 after the second trimming. Calibration was performed to ensure that a lack of fusion connected to the surface (positive in penetrant testing) produced a vertically oriented signal phase, resulting in a blue indication. For non-surface-breaking indications, the signal phase rotated due to the skin effect delay, resulting in a red shift. The color variation was proportional to the ligament depth.

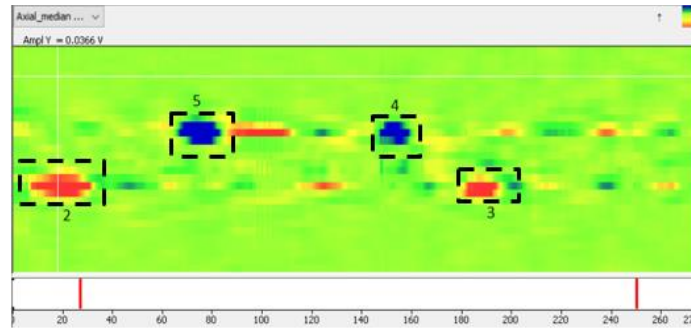


Figure 7. C-Scan ECA at 20 kHz of specimen 309-1 after 2 mm trim; Surface-Connected (blue) and Non-open (red) fusion defects.

The results were analyzed in three stages:

1. Comparison of eddy current detection with PT.
2. Calculation of detection probability as a function of defect length.
3. Verification of detection for LOF not connected to the surface.

The detection efficiency was evaluated using the 3 mm ECA probe at 75 kHz. The results for plate 309L-2 are shown in Table 3, presented in stratigraphic format. A yellow cell indicates that both the ECA probe and dye penetrant testing produced positive results at the locations of fusion gaps. A strong correlation was observed for the 309L (non-ferromagnetic) filler material, while several indications with 410NiMo filler metal produced negative eddy current results. The detection rate for 309L filler material was 48/50 (96%), whereas for 410NiMo it was 11/17 (65%). The difference in detection rates between 309L and 410NiMo was not investigated in depth; however, defects in 410NiMo welds were generally smaller and tighter than those in 309L, making LOF in 410NiMo more challenging to both manufacture and detect.

A correlation was established between the length of penetrant indications – that we consider as the defect size - and the probability of detection (POD) using the 3 mm ECA probe. The data were analyzed using MH1823 software [15], resulting in a POD curve for surface-connected LOF as a function of defect length. The calculated defect length corresponding to a 90% detection probability was 8.24 mm, as shown in Figure 8. Most ECA-negative indications had lengths of 3 mm or less.

Table 3. Stratigraphic Detection with 3 mm ECA Array at 75 kHz for Sample 309L-2 (Plate 415)
 (Yellow cells indicate ET and PT detection; red cells indicate PT only; NDD refers to indications that are not detectable).

layer	Presence of indication				
	Ind. 1	Ind. 2	Ind. 3	Ind. 4	Ind. 5
1	NDD	NDD	NDD	X	X
2	NDD	NDD	NDD	X	X
3	NDD	NDD	NDD	X	X
4	NDD	NDD	X	X	X
5	NDD	NDD	X	X	X
6	NDD	NDD	X	X	X
7	NDD	X	X	NDD	X
8	NDD	X	X	X	X
9	NDD	X	X	X	X
10	NDD	NDD	NDD	NDD	X
12	NDD	NDD	NDD	NDD	X
14	NDD	NDD	NDD	NDD	X

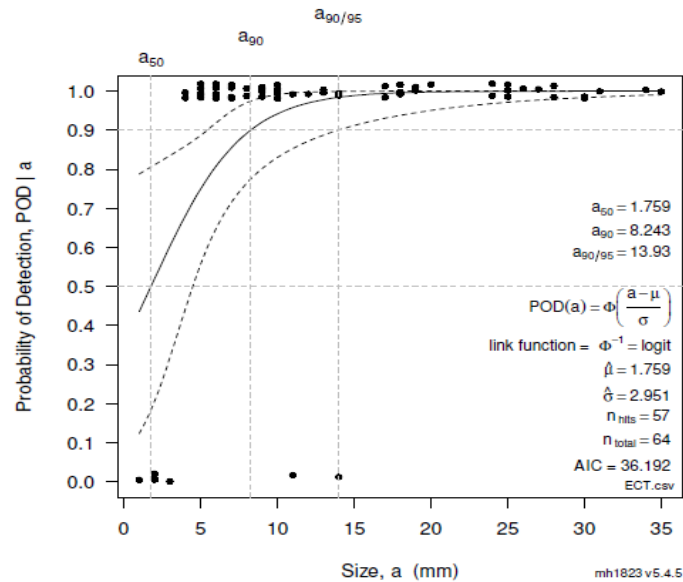


Figure 8. POD Hit/Miss curve using MH1823 Software for 3 mm ECA Probe Detection as a Function of Penetrant Indication Length

To detect LOF not connected to the surface, data from the 5 mm ECA probe at 20 kHz were analyzed. The detection rate was 7/8 (87%) in 309L and only 1/9 (11%) in 410NiMo, reflecting the limited penetration depth in the ferromagnetic 410NiMo material. Detection using the orthogonal probe produced better results, with only one penetrant indication missed, resulting in a detection rate of 66/67 (98%). The missed indication was considered an outlier. The POD calculation could not be performed with the orthogonal probe data, as the dataset included only one missed flaw, resulting in an almost horizontal POD curve. The detection results indicate that

the orthogonal probe successfully detected defects as short as 1.5 mm. No discrepancies were observed between PT and the orthogonal probe, suggesting that both methods yield essentially the same sensitivity to linear surface-breaking defects. Based on these findings, the following conclusions can be drawn for Eddy current inspection:

- Eddy current inspection, particularly with the orthogonal probe, is highly effective for detecting surface-connected LOF and demonstrates equal effectiveness for both 410NiMo and 309L materials.
- Non-surface-breaking LOF in 309L can be detected using an ECA probe at low frequencies, with potential for identifying volumetric defects within the 309L filler weld. However, this method is not suitable for 410NiMo welds, as the detection rate is significantly lower.

3.3. Ultrasound testing results

Ultrasonic testing was performed using three array techniques, two vibration modes, and two frequencies. A matrix of four welded samples was created using two base materials and two filler materials. The complexity of the analysis arises from the wide range of ultrasonic and material variables. A common factor across all samples is that the base material is martensitic steel, while the filler metals are approved for repairs on martensitic Francis runners. The analysis is structured to first present the results for each base material, followed by categorization based on inspection techniques. Calibration was consistent across all array techniques. A 410-calibration block with a 1.5 mm side-drilled hole (SDH) was used to calibrate sensitivity, employing time-corrected gain (TCG) for inspecting plates made from 410 base material [6]. For the 415 base material, an AWS steel block was used for calibration due to the similarities in attenuation and velocity between the two materials. Amplitude was normalized to 80% of the full screen height (FSH) for the required metal path covering the repaired volume. The detection threshold was set at -11 dB from the reference, in accordance with the CSA W59 code for ultrasonic testing of dynamically loaded structures [16]. This -11 dB threshold was uniformly applied as the detection criterion across all array techniques.

3.3.1. Sample 410 Base Material

The inspection of the 410 base material yielded satisfactory detection results, despite the material exhibiting acoustic anisotropy and a higher attenuation coefficient compared to the 415 base material. The overall results are summarized in Tables 4 and 5.

For the 309L filler material, all LOF defects were detected across all techniques, modes, and frequencies. The weakest signal recorded was -10 dB using the TFM method in shear wave mode at 2.25 MHz. Overall, the TFM method consistently produced weaker responses compared to beamforming methods. A notable observation is that shear wave inspection at 5 MHz was unsuitable for this sample. Flaw responses appeared distorted compared to compression wave results, and non-relevant indications were observed, as shown in Figure 10. However, the TFM compression wave at 5 MHz provided responses that closely matched the penetrant testing (PT) results. Despite these challenges, all relevant indications were successfully detected using the 5 MHz shear wave.

Table 4. Plate 410 with 309L filler (Maximum flaw amplitude in dB)

Methods	Freq. (MHz)	Wave Mode	Ind.1	Ind.2	Ind.3	Ind.4	Ind.5
PT (Flaw size)			4x55	3x13	5x10	3x10	3x15
TFM	5	LW	-4	-8	-4	-8	-6
PAUT Compound (40-70)	5	LW	3	0	3	4	2
PAUT Linear 60	5	LW	3	5	4	5	3
TFM	5	SW	2	-5	-5	-4	-2
PAUT Compound (40-70)	5	SW	9	-1	0	2	6
PAUT Linear 60	5	SW	9	0	-2	2	5
TFM	2.25	SW	2	-10	-6	-10	-5
PAUT Compound (40-70)	2.25	SW	11	3	5	5	10
PAUT Linear 60	2.25	SW	14	4	1	4	10

Note: The detection threshold is set to -11 dB (All technique/mode/frequency detected all manufactured flaws).

Anisotropy was observed during shear wave inspection of plate 410 with 309L filler metal. In Figure 9, Figure (a) shows the response of flaws #2 and #3 using TFM with a 5 MHz compression wave (LW). The flaws exhibit distinct ultrasonic responses with minimal grain noise. The PT results are overlaid as magenta lines on the ultrasonic image. Figure (b) displays the results using TFM with a 5 MHz shear wave (SW). In this case, flaws #2 and #3 appear elongated in the vertical plane, non-relevant indications are present between flaws #2 and #3, and the grain noise is more pronounced.

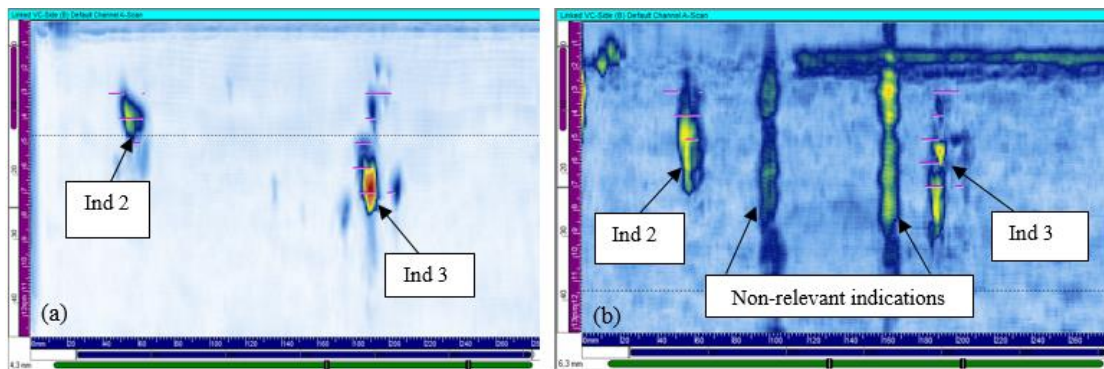


Figure 9. TFM Results for Plate 410 with 309L Filler Material; (a) LW at 5 MHz showing clear flaw details, and (b) SW at 5 MHz showing distorted signals and non-relevant indications; Vertical magenta lines represent the PT results.

For the 410NiMo filler, the detection amplitude was reduced compared to the 309L filler sample. This reduction can be attributed to the smaller flaw sizes in this sample. The smallest flaw, measuring 1×2 mm, was detected in 4 out of 9 configurations. Consistent with previous observations, the TFM method produced the lowest amplitude response, and indication #2 (2×9 mm) was missed in shear wave mode. However, shallow flaws, indications #4 and #5, were detected with a satisfactory amplitude margin of approximately 11 dB. These two lack-of-fusion flaws (#4 and #5) were measured using PT at 1×10 mm and 1×12 mm, respectively, which fall within the lower range for flaw height.

Table 5. Plate 410 with 410NiMo filler (Maximum flaw amplitude in dB).

Methods	Freq. (MHz)	Wave Mode	Ind.1	Ind.2	Ind.3	Ind.4	Ind.5
PT (Flaw size)			3x20	2x9	1x2	1x10	1x12
TFM	5	LW	-7	-6	ABT(-16)	-4	-1
PAUT Compound (40-70)	5	LW	-10	-6	ABT(-17)	-1	0
PAUT Linear 60	5	LW	0	-5	-11	0	-2
TFM	5	SW	-7	NDD	NDD	-9	0
PAUT Compound (40-70)	5	SW	-2	-3	-10	-3	2
PAUT Linear 60	5	SW	3	-5	ABT(-12)	6	0
TFM	2.25	SW	-8	ABT(-14)	ABT(-16)	-11	-9
PAUT Compound (40-70)	2.25	SW	-4	-3	-5	0	1
PAUT Linear 60	2.25	SW	-1	-2	-4	0	2

Note: The detection threshold is set to -11 dB. Some flaws were missed (ABT is for amplitude below detection threshold).

3.3.2. Sample 415 Base Material

The inspection of the 415 base material proved more challenging for detecting lack of fusion (LOF) compared to the 410 base material. The overall results are summarized in Tables 6 and 7. For the 309L filler material, the peak amplitude measured was generally satisfactory, though in some cases, the detection margin was reduced to approximately 2–4 dB. For flaws of similar size, the ultrasonic response was noticeably weaker compared to that of the 410 base material. Additionally, the results for the 5 MHz shear wave were found to be unreliable, with only the deeper defects (indications #4 and #5) being detected, yielding a margin of 17 dB.

Table 6. Plate 415 with 309L filler (Maximum flaw amplitude in dB).

Methods	Freq. (MHz)	Wave Mode	Ind.1	Ind.2	Ind.3	Ind.4	Ind.5
PT (Flaw size)			----	3x9	3x14	9x16	16x27*
TFM	5	LW	-6	-9	-8	4	4
PAUT Compound (40-70)	5	LW	-6	-6	-9	12	12
PAUT Linear 60	5	LW	-5	-7	-6	12	12
TFM	5	SW	ABT(-21)	ABT(-14)	ABT(-17)	ABT(-12)	-10
PAUT Compound (40-70)	5	SW	ABT(-18)	-9	ABT(-14)	6	6
PAUT Linear 60	5	SW	NDD	ABT(-14)	ABT(-16)	6	6
TFM	2.25	SW	-8	-7	-7	-5	-4
PAUT Compound (40-70)	2.25	SW	-10	-6	-4	12	12
PAUT Linear 60	2.25	SW	-6	-5	-3	12	12
*Surface breaking							

Note: The detection threshold is set to -11 dB. Shear wave at a frequency of 5 MHz proved unreliable for this sample. LOF #4 and #5 cracked during the straightening process and indication #5 is surface breaking.

For the 410NiMo filler material, the peak amplitude measured was below the detection threshold in most cases. The PT results indicate that all flaw heights are either 1 or 2 mm, which may explain the challenges the ultrasonic array method faces in detecting these lack of fusion (LOF) defects.

The TFM results, shown in Figure 10, demonstrate that the ultrasonic responses for indications #2, #4, and #5 are very weak, falling well below the detection threshold. This observation raises a critical question: could the 410NiMo filler material, with the applied welding parameter variations, exhibit a reduced tendency to form fusion defects?

A comparative analysis of flaws #2 to #5 in samples 410/410NiMo and 415/410NiMo reveals that PT identified similar flaw sizes in both samples. However, with the ultrasonic array technique, the detection rate—considering all configurations—is 29 out of 36 (80%) for the 410/410NiMo sample and only 7 out of 36 (19%) for the 415/410NiMo sample. This discrepancy strongly suggests an influence from the metallurgical properties and the flaw formation mechanism. The

compactness of the LOF defects in sample 415/410NiMo may be the primary reason for the weak amplitude signals observed.

Table 7. Plate 415 with 410NiMo filler (Maximum flaw amplitude in dB).

Methods	Freq. (MHz)	Wave Mode	Ind.1	Ind.2	Ind.3	Ind.4	Ind.5
PT (Flaw size)			-----	2x7	1x18	1x8	2x8
TFM	5	LW	-7	ABT(-20)	ABT(-14)	ABT(-20)	ABT(-17)
PAUT Compound (40-70)	5	LW	-8	ABT(-18)	ABT(-14)	ABT(-15)	-10
PAUT Linear 60	5	LW	-9	ABT(-18)	ABT(-13)	ABT(-14)	-9
TFM	5	SW	-7	NDD	ABT(-21)	NDD	ABT(-18)
PAUT Compound (40-70)	5	SW	1	ABT(-20)	ABT(-18)	ABT(-21)	ABT(-13)
PAUT Linear 60	5	SW	-11	ABT(-21)	ABT(-17)	ABT(-16)	-8
TFM	2.25	SW	0	NDD	NDD	ABT(-20)	ABT(-13)
PAUT Compound (40-70)	2.25	SW	2	ABT(-19)	-8	ABT(-18)	-9
PAUT Linear 60	2.25	SW	3	NDD	-9	ABT(-14)	-8

Note: The detection threshold is set at -11 dB. Only indication #1 in the root area was reliably detected across all methods, frequencies, and modes. Indications #2, #3, #4, and #5 were smaller and showed weaker ultrasonic responses compared to PT results.

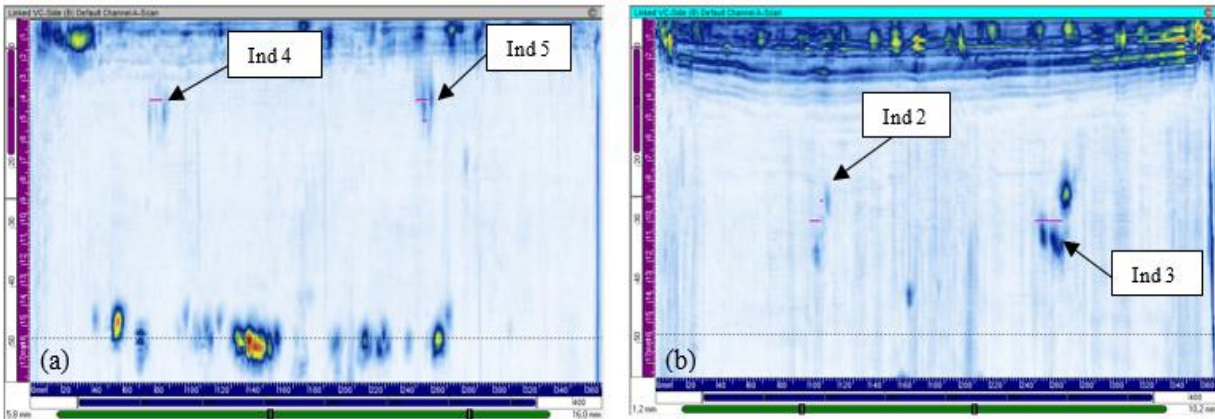


Figure 10. TFM response at 5 MHz for Plate 415 with 410NiMo Filler metal (a) Compression Wave at Skew 90 (b) Compression Wave at Skew 270 (Vertical magenta lines represent the PT results).

3.3.3. Statistical study

A statistical analysis of all sample results was conducted to compare detection methods, wave modes, and frequencies. The detection rate for each method, considering all wave modes and frequencies as a function of base material, is presented in Table 8. As discussed in the previous section, the 415 base material proved more challenging for detecting LOF in weld repairs compared to the 410 material. Beamforming techniques achieved a 97% detection rate in the 410 material but only 60% in the 415 material. Furthermore, beamforming techniques demonstrated a higher detection rate than TFM under identical calibration parameters.

Table 8. Detection rate as a function of plate and technique.

Methods	415/309L	415/410NiMo	Rate (415)	410/309L	410/410NiMo	Rate (410)
TFM	11	3	0.47	15	10	0.83
Compound	12	6	0.60	15	14	0.97
Linear 60	12	7	0.63	15	14	0.97
Total	35	16	0.57	45	38	0.91

Note: Wave mode and frequency are consolidated. Each method includes three mode/frequency configurations and five flaws, total 15 cases per method.

The primary objective of this study is to validate the suitability of ultrasonic array techniques for detecting weld flaws in shallow repairs. Table 9 summarizes the detection results based on flaw depth, categorized into two groups: flaws in the weld pass closest to the surface and flaws in the 2nd or 3rd pass. Flaws near the surface were detected across all configurations in material 410, whereas only 28% were detected in material 415. For flaws in the center passes, the detection rate decreased to 81% for material 410 and 42% for material 415. These results indicate that material 410 is a suitable candidate for ultrasonic array techniques to identify lack of fusion in shallow repairs, whereas material 415 appears less reliable for this inspection purpose.

Table 9. Detection rate per base material and depth of lack of fusion (9 configurations and 4 flaws produce 36 cases)

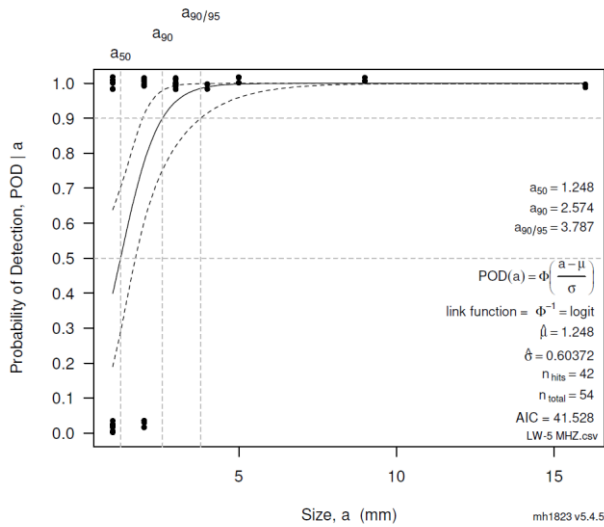
Base Material	Flaws x configurations detection in Last Pass (nb)	Flaws x configurations in Last Pass (Total)	Detection in Last Pass (Rate)	Flaws x configurations detection in Center Pass (nb)	Flaws x configurations in Center Pass (Total)	Detection in Center Pass (Rate)
410	36	36	1.00	29	36	0.81
415	5	18*	0.28	15	36	0.42

* Two LOF that cracked during straightening are excluded.

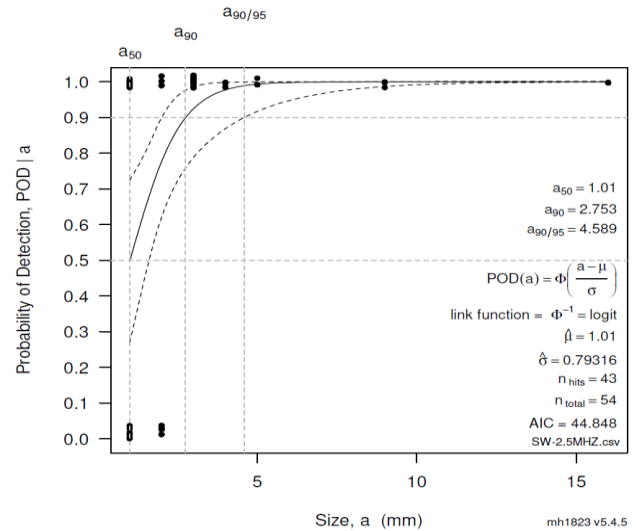
Using the lack of fusion (LOF) size determined by stratigraphic PT measurements (red penetrant leaking indication size), the UT array data were processed to compute Probability of Detection (POD) curves as a function of wave mode and frequency. UT array data from TFM, PAUT compound, and linear scans were combined to analyze the detection of known LOF heights. POD curves for the hit/miss algorithm, generated using MH1823 software, are shown in Figure 11. The LOF height required to achieve a 90% probability of detection is 2.574 mm for a 5 MHz compression wave, 2.753 mm for a 2.25 MHz shear wave, and 7.762 mm for a 5 MHz shear wave, as presented in Table 10. The first two mode/frequency combinations demonstrated very similar detection capabilities for embedded LOF in repairs on martensitic steel.

Table 10. Results of Pod calculations for different wave mode

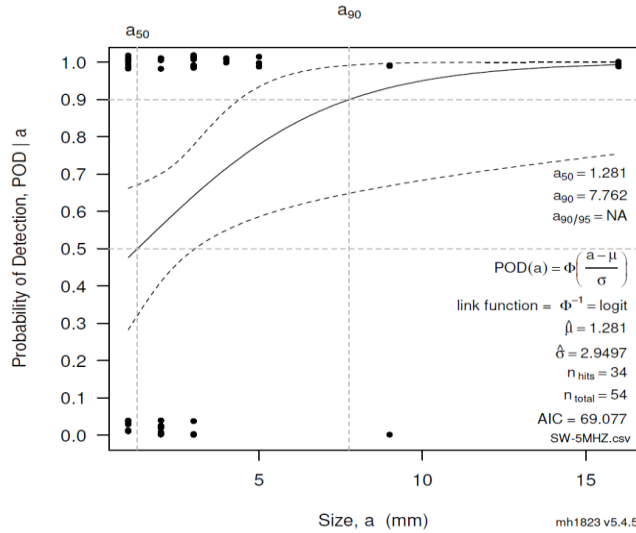
Wave type and frequency	a50 (mm)	a90 (mm)	a90/95 (mm)
Longitudinal wave (5 MHz)	1.24	2.57	3.78
Shear wave (5 MHz)	1.28	7.76	NA
Shear wave (2.25 MHz)	1.01	2.75	4.58



(a) POD curve for longitudinal wave at 5 MHz



(b) POD curve for shear wave at 2.25 MHz



(c) POD curve for shear wave at 5 MHz

Figure 11. POD curves by mh1823 software; All UT array techniques results merged as function of wave mode and frequency (The horizontal axis is flaw height).

4. Recommended inspection techniques for repairs

To identify the most suitable inspection techniques, it is essential to consider factors that impact the outcomes of an ultrasonic inspection, including:

- **Sub-surface Resolution:** The TFM mode at 5 MHz with a compression wave offers excellent resolution for near-surface defects. The region of interest lies beneath the front of the wedge. The detection limit is constrained by physical principles, specifically the wavelength, which in this case is 1.12 mm, enabling the detection of ligaments approximately 1 mm in size.
- **Detection Rate:** For defects positioned deeper below the surface, a 2.25 MHz shear-wave beamforming technique provides optimal results. However, this approach has limitations in terms of sub-surface resolution.
- **Calibration:** Calibration poses challenges in beamforming mode when using compression waves, as phantom echoes from the shear component can interfere. This issue is mitigated in TFM mode, where the LL computed path effectively filters out the shear component, and vice versa.
- **Accurate Sizing:** Although flaw sizing data is not presented in this paper, the TFM 5LW mode produced sizing results most closely aligned with PT measurements.

- **Contact Surface:** A 64-element probe with a footprint of 28×57 mm is recommended for repair sites sufficiently distant from any edge, allowing for a complete 360° rotation of the probe to inspect the fusion surface. For indications near an edge, a 16-element probe in beamforming mode with a footprint of 30×25 mm allows for closer manipulation near the edge.
- **Surface Flatness:** If the area surrounding the repair is not flat, a smaller wedge combined with a 16-element probe in beamforming mode will provide improved contact.

In summary, the recommended techniques for repair inspection are as follows:

1. TFM: 64-element probe, 5 MHz compression wave.
2. Azimuthal or compound: 64-element probe, 2.25 MHz shear wave.
3. Azimuthal or compound: 16-element probe, 2.25 MHz shear wave.

5. Conclusions

The effectiveness of repair inspections using the eddy current technique has been clearly demonstrated in this study. Notably, the use of an ECA probe at a low frequency enables the detection of non-through fusion defects when the filler metal is 309L. The detection probability reaches up to 90%, depending on the indication length—8.24 mm in ECA mode and 1.5 mm with an orthogonal probe.

Ultrasound testing has also proven to be a reliable tool for inspecting repairs. Given that repair depths may only be a few millimeters, a method with high sub-surface resolution is essential. The TFM imaging technique fulfills this need, enabling near-surface inspections when the calculation zone is positioned beneath the wedge's front. The sub-surface resolution limit is approximately on the order of the wavelength, around 1.1 mm for the 5 MHz LW mode. In cases where eight defects were positioned near the surface, beamforming techniques successfully detected seven, meeting the W59 standard's acceptance criteria.

For repairs distant from the trailing edge or other interfaces, a 64-element, 5 MHz transducer paired with a compression-mode wedge is recommended. Conversely, for curved inspection surfaces or repairs near edges, a 16-element, 2.25 MHz transducer with a shear-mode wedge is more suitable.

Detection rates relative to lack of fusion (LOF) height are approximately 50% for heights in the 1–2 mm range, increasing to nearly 100% for heights exceeding 3 mm. These results align with other POD studies conducted on CA6NM or 415 martensitic base material [1-3, 6]. The precision of flaw dimensioning is noteworthy, matching the wavelength order—approximately 1 mm in height and 3 mm in width, excluding the two identified cracks.

An area for further investigation is the scanning of indications. Inspection protocols should provide clear guidelines for marking the repaired area on the component, potentially utilizing eddy currents with 309L, and for thoroughly examining the fusion surface. Repair examinations should be conducted freehand, with the operator positioning the probe to ensure the TFM calculation zone or beam incidence achieves an optimal reflection angle on the repair interface. Scans must cover the entirety of the repair's wall and fusion volume.

If the repair is located at the weld joint, fully scanning the repair surface presents a challenge, as a flat shoe restricts 360° probe rotation. Alternative strategies, such as using a 2D array, should be explored. To ensure effective inspections, rigorous inspector training and validation of proficiency are essential.

Acknowledgment

This project was made possible through the invaluable support of the Quebec Metallurgy Center (CMQ), which generously provided the facilities, inspection equipment, and tools necessary for plate fabrication. We extend our sincere appreciation to Théo Ouellet for his significant contributions to the design and welding of the plates. Furthermore, we acknowledge the expertise and active involvement of Yves Tremblay in the eddy current inspection throughout the project.

References

1. Bajgholi, M. (2023). Advanced ultrasonic inspection technologies applied to the welded joints of hydraulic turbine runners (Doctoral dissertation, École de technologie supérieure).
https://espace.etsmtl.ca/id/eprint/3196/1/BAJGHOLI_Mohammadebrahim.pdf.
2. Bajgholi, M. E., Rousseau, G., Viens, M., & Thibault, D. (2021). Capability of advanced ultrasonic inspection technologies for hydraulic turbine runners. *Applied Sciences*, 11(10), 4681. <https://doi.org/10.3390/app11104681>.
3. Bajgholi, M. E., Rousseau, G., Viens, M., Thibault, D., & Gagnon, M. (2023). Reliability assessment of non-destructive testing (NDT) for the inspection of weld joints in the hydroelectric turbine industry. *The International Journal of Advanced Manufacturing Technology*, 128(9-10), 4223-4233. <https://doi.org/10.1007/s00170-023-12176-5>.

4. Stenberg, T., Barsoum, Z., Åstrand, E., Öberg, A. E., Schneider, C., & Hedegård, J. (2017). "Quality control and assurance in fabrication of welded structures subjected to fatigue loading", *Welding in the World*, 61, 1003-1015. <http://dx.doi.org/10.1007/s40194-017-0490-5>
5. Panthee, A., Thapa, B., & Neopane, H. P. (2015), "Quality control in welding repair of Pelton runner. *Renewable Energy*", 79, 96-102. <https://doi.org/10.1016/j.renene.2014.10.042>.
6. Bajgholi, M. E., Rousseau, G., Viens, M., & Thibault, D. (2023). Advanced ultrasonic inspection methodologies for fitness-for-service (FFS) assessment of hydraulic turbines. *The International Journal of Advanced Manufacturing Technology*, 129(5), 2621-2633. <https://doi.org/10.1007/s00170-023-12498-4>.
7. Machado, M. A. (2024). Eddy currents probe design for NDT applications: A review. *Sensors (Basel, Switzerland)*, 24(17), 5819. <https://doi.org/10.3390/s24175819>.
8. Krause, T. W., & Underhill, P. R. (2019). Selecting the correct electromagnetic inspection technology. *Adv. Mater. Lett*, 10(7), 441-448. DOI: 10.5185/amlett.2019.2262.
9. Bajgholi, M. E., Rousseau, G., Ginzl, E., Thibault, D., & Viens, M. (2023). Total focusing method applied to probability of detection. *The International Journal of Advanced Manufacturing Technology*, 126(7), 3637-3647. <http://dx.doi.org/10.1007/s00170-023-11328-x>
10. Bajgholi, M. E., Viens, M., Rousseau, G., Ginzl, E., Thibault, D., & Gagnon, M. (2024). "Ultrasonic Testing Techniques for Integrity Assessment of Hydraulic Turbine Runner". *The ReJNDT special issue 'Frontiers in Non-destructive Testing and Evaluation: Academic Insights'*. <https://www.ndt.net/?id=29363>.
11. Bajgholi, M. E., Rousseau, G., Ginzl, E., Viens, M., & Mélançon, V. (2024). Developing flaw sizing methodology in Total Focusing Method (TFM) by EDM calibration blocks. <https://www.ndt.net/?id=30295>.
12. ASTM, ASTM E165/E165M – 23, Standard Practice for Liquid Penetrant Testing for General Industry, 2023, Pennsylvania: ASTM International. DOI: 10.1520/E0165_E0165M-23.
13. ASTM, ASTM E 494 Standard Practice for Measuring Ultrasonic Velocity in Materials, 2023, Pennsylvania: ASTM International (2015). DOI: 10.1520/E0494-15.
14. Bellemare, J., Hassanipour, M., Godin, S., Rousseau, G., & Pouliot, N. (2023). Validation through field data of LineCore, a lightweight Eddy-current sensor for the early detection of corrosion of ACSR. <https://doi.org/10.58286/28196>.
15. Annis C, Statistical best-practices for building probability of detection (POD) models. (2022) , R package mh1823, version 5.4.5. <https://statistical-engineering.com/mh1823-history/>
16. Canadian Standards Association (CSA) (2013) CSA W59–13 Welded Steel Construction (Metal Arc Welding). Mississauga, ON, Canada.